Effects of NaF evaporation during low temperature Cu(In,Ga)Se_2 growth

B. Bissig*, P. Reinhard, F. Pianezzi, H. Hagendorfer, S. Nishiwaki, S. Buecheler, A.N. Tiwari

Laboratory for Thin Films and Photovoltaics, Empa, Swiss Federal Laboratories for Materials Science and Technology, Ueberlandstrasse 129, 8600 Duebendorf, Switzerland.

*Corresponding author: phone: +41 58 765 43 05, fax +41 58 765 1112, e-mail: benjamin.bissig@empa.ch

ABSTRACT

Co-evaporation of NaF during the 3rd stage of the low temperature Cu(In,Ga)Se_2 multi-stage process is compared to post deposition treatment (PDT) with NaF in view of their influence on the electronic and structural properties. In case of NaF co-evaporation, quantum efficiency losses in the near infrared region and thus lower short circuit current density cause a reduced efficiency compared to solar cells prepared with NaF PDT. The formation of a deep defect with activation energy of ~250 meV is measured by capacitance spectroscopy and can explain the deteriorated performance in such devices. In addition, NaF co-evaporation during the 3rd stage causes reduced grain size in the top part of Cu(In,Ga)Se_2 and altered In, Ga and Cu distribution.

Keywords: CIGS, PDT, admittance spectroscopy, alkali, sodium, SIMS, ICPMS

1. INTRODUCTION

Alkali elements and the way they are introduced in $Cu(In,Ga)Se_2$ (CIGS) layers play a recurring role in the efficiency improvement of solar cells. The necessity to add dilute amounts of alkali elements to the CIGS layer is known for more than two decades [1]. Traditionally they have been incorporated by diffusion at high temperature from soda lime glass (SLG) substrates during CIGS growth. In case of alkali free substrates such as polyimide (PI) co-evaporation or precursor strategies were first investigated [2-6]. Despite its well-known beneficial effects on device properties Na was found to decrease CIGS grain size [4, 6], reduce the minority carrier lifetime [7], and affect the Cu and Ga distribution when added during absorber growth [4, 6]. It was also realized by our group that the beneficial effects of Na on electronic properties can be effectively isolated from its effect on CIGS growth properties by a post deposition treatment (PDT) with NaF [8].

CIGS for highly efficient solar cells is often grown by a 3-stage process. In the 1st stage In and Ga are co-evaporated together with Se. During the 2nd stage Cu and Se are added until a Cu rich composition is achieved. Finally, in the 3rd stage, In, Ga, and Se are supplied again until an overall Cu poor absorber is reached. Our group reported that addition of NaF during the 3rd CIGS deposition stage yields similarly efficient solar cells as compared to NaF PDT, whereas addition of NaF during the 1st and 2nd stage [5] typically leads to lower PV performance.

In a previous study we showed that KF co-evaporation during the 3rd stage induces the formation of a deep defect, which is absent when KF is added by a PDT, and discussed its effects on electronic properties [11]. To investigate to what extend this also happens when NaF is co-evaporated, and as an attempt to further increase the carrier concentration while avoiding the unfavorable effects of early Na incorporation, we focus on NaF co-evaporation during the 3rd stage after a Cu-poor composition is reached. Therefore, in the following we compare NaF co-evaporation to a PDT

approach with respect to effects on electronic and compositional device properties while keeping the total amount of supplied NaF fixed in all cases.

2. EXPERIMENTAL DETAILS

CIGS solar cells were deposited on Mo coated PI substrates. The ~2.5 µm thick absorbers were grown by co-evaporation at a maximum substrate temperature of 450°C in a high vacuum chamber equipped with an additional NaF effusion cell. A modified 3-stage process (multi-stage process) similar to the one described in [8] was used. Final [Cu]/([Ga]+[In]) (CGI) values determined by XRF range between 0.78 and 0.82 and the [Ga]/([Ga]+[In]) (GGI) ratios are between 0.36 to 0.38. NaF was evaporated either during the whole 3rd stage (5'-20'), or only for a reduced time (5'-11') but with a higher rate, see Fig. 1, at a substrate temperature of 450 °C. During the PDT NaF was evaporated for 20 min at a substrate temperature of ~350 °C, as described in [8]. The total flux of NaF is similar in all cases. Solar cells were finished with a CdS buffer layer, an i-ZnO/ZnO:Al front contact, a metal grid and anti-reflective coating following our standard recipe [12] .

Figure 1

The photovoltaic (PV) parameters of the solar cells were extracted from current density-voltage (J-V) characteristics under simulated standard test conditions (1000 W/m^2, 25 °C, AM1.5G) measured with a Keithley 2400 source meter with four terminal sensing. External quantum efficiency (EQE) curves were obtained using a lock-in amplifier from Stanford Research Systems and chopped light from a halogen lamp. An Agilent E4980A LCR meter was used for capacitance-frequency (C-f) and capacitance-voltage (C-V) measurements. C-f, C-V as well as illumination dependent J-V measurements were performed in the range from 120 K to 340 K in a cryostat cooled with liquid nitrogen. All capacitance measurements were performed in relaxed state, i.e. devices were stored for at least 30 min in dark before cooling. Reverse saturation current density j_0, its activation energy E_{j0}, and the diode ideality factor A were extracted from illumination and temperature dependent J_{SC}-V_{OC}

measurements, as described in [13]. Elemental depth profiles were performed with time-of-flight secondary ion mass spectrometry (ToF-SIMS5, ION-TOF) and for quantification of Na in CIGS inductively coupled plasma mass spectrometry (ICP-MS) was used. Experimental details are given elsewhere [8]. Scanning electron microscopy (SEM) was performed in a Hitachi S-4800 SEM at 5 keV acceleration voltage and a working distance of 5.2 mm.

3. RESULTS

3.1 Effects on composition and morphology

Figure 2

Fig. 2 compares Na, In, Ga and Cu elemental depth profiles in the top 350 nm of the CIGS layer through completed devices where Na was introduced after (PDT) or during (5'-11' and 5'- 20') the 3rd deposition stage after the layer becomes Cu-poor. The time window where NaF was co-evaporated is reflected in the Na profile close to CdS/CIGS interface with a Na count rate up to ~2 orders of magnitude higher relative to the PDT treated sample. A spiked Na signal is observed in the 5'-11' case whereas the count rate appears more plateau like in the 5'-20' case. The absolute Na concentrations with respect to the CIGS layer as measured by ICP-MS are given in Table 1. For the two absorbers with co-evaporated NaF the Na content is roughly one order of magnitude higher compared to the PDT sample. The SEM micrograph in Fig. 3 shows the cross section of the NaF PDT and 5'-20' sample. A significant decrease in grain size is observed in the top region of the absorber when NaF is co-evaporated instead of a PDT. Atom probe tomography of CIGS layers revealed that Na resides mainly at grain boundaries [14, 15] which can explain the higher absolute Na content and the increased SIMS Na count rate with respect to CIGS in our samples. Similar effects on grain size and SIMS profiles were previously reported in case of NaF [2-6] and KF [11] co-evaporation.

Figure 3

3.2 Effects on electronic properties

Table 1 compiles the PV parameters of the solar cells with the three different absorbers. Na introduction during the 3rd deposition stage decreases the cell efficiency with respect to PDT. This loss is mainly caused by a decrease in short circuit current (J_{SC}) and fill factor (FF). The diode ideality factor, $j_0$and E_{j0} do not indicate a clear difference in recombination mechanism for the three cases. All E j_0 are close to Eg ~1.15 eV and the ideality factors are about ~1.4, indicating recombination in the space charge region. Furthermore, a decreasing JSC was observed at low temperatures (not shown).

Figure 4

EQE curves are shown in Fig 4. An overall reduction in EQE is observed when NaF was present during CIGS deposition. Further, the 5'- 20'sample suffers from increased losses in the near infrared (NIR) region. Typically such NIR losses arise due to short minority carrier diffusion length or due to incomplete absorption. Given the comparable GGI values and similar absorber thickness we will discuss our results in terms of a defect related model in the following.

To access the defect structure C-f spectra were recorded at temperatures between 120 K and 300 K (Fig. 5). All samples feature a typical response often referred to as N1 signal at low temperature [16] with a characteristic energy of 110-140 meV but no further deep defects are observed in case of NaF PDT. The NaF co-evaporated samples exhibit another pronounced capacitance step at low frequencies and higher temperature which can be interpreted as capacitance contribution from inter-band defect states. A rescaling of the C-f profiles as described in [17] allows extracting their activation energy which is found to be 250 meV, similar to the value reported for KF in [11].

Low temperature (< 200 K) C-V profiling at a frequency of 300 kHz was used to estimate the shallow carrier density N_{CV} of the absorbers (see table 1). For samples without any NaF supply carrier densities N_{CV} of 1 x 1014 cm^{-3} were reported [10]. Compared to this, the PDT and NaF co-evaporation treatments increased N_{CV} to 2 x 1015 cm^{-3} and ~1 x 1016 cm^{-3}, respectively. We note that, the

increased N_{CV} cannot be directly attributed to the way of Na incorporation but is more likely an effect of the higher amount of Na in CIGS when NaF is added by co-evaporation (see Table 1).

4. DISCUSSION

The observations presented above support that Na presence during CIGS deposition induces the formation of a deep defect with an activation energy of 250 meV. An increased recombination across this defect in the region close to the interface can account for the broadband reduction of EQE. We reported the formation of a similar defect and a similar electronic behavior in case of KF co-evaporation during the 3rd stage [11]. This is a strong support that both alkali elements can induce the formation of a similar defect type when evaporated at comparable amounts as in a PDT during the growth process. At the moment it is not possible to differentiate if this deep defect level is due to the presence of the alkali element as interstitial or substitutional element like Na_{Se} [18] in the CIGS crystal, or if its presence induces the formation of intrinsic defects like Cu_{In} or Cu_{Ga} [19] due to different migration of the metals in the presence of Na. Further, the appearance of this defect could be related to the increased density of grain boundaries or could be an impedance response caused by the microstructural change. This cannot be excluded as up to date no reports that correlate grain size to measured capacitances are available.

Earlier work on CIGS showed a beneficial effect of Na on V_{OC} and FF which is usually attributed to increased net carrier concentration. Here, despite increased N_{CV} the V_{OC} was found to remain unchanged and the FF decreased in the case of co-evaporation as compared to the PDT. This can be understood as in case of bulk recombination the j_0 and thus V_{OC} depend on carrier concentration as well as diffusion length [20]. Therefore, despite increased carrier concentration the V_{OC} can be limited by the structural degradation of the surface near region and by the observed electrically

active defect as both can explain a shorter minority diffusion length by the reduction of mobility or lifetime, respectively.

5. CONCLUSIONS

NaF co-evaporation during the 3rd CIGS deposition stage was found to cause a deep defect like C-f response with an activation energy of 250 meV. This signal appears in addition to the N1 response which is also observed for the PDT sample. A decreased EQE and a higher carrier density were observed in devices with NaF co-evaporation relative to NaF PDT. Further, NaF co-evaporation locally increases the relative Na content which is assumed to be due to reduced grain size. Our findings thus show that the consequences of NaF co-evaporation on electronic behavior are similar to that observed for KF co-evaporation during the 3rd stage [11], although somewhat less pronounced. The formation of a deep defect like response and the effects on morphology and elemental composition all indicate that during the low temperature processes the presence of high amounts of alkali elements should be avoided. Thus, post deposition treatments and alkali free substrates seem favorable as compared to the co-evaporation of comparable amounts of alkali elements.

ACKNOWLEDGEMENTS

The Laboratory for Analytical Chemistry and the laboratory for Nanoscale Materials Science at Empa are acknowledged for providing access to ICP-MS and SIMS instrumentation, respectively. Financial support from the Swiss national science foundation (project Nr. 200021_149453 / 1) and the FP7 R2R-CIGS project (project Nr. 283974) is gratefully acknowledged.

List of figures:

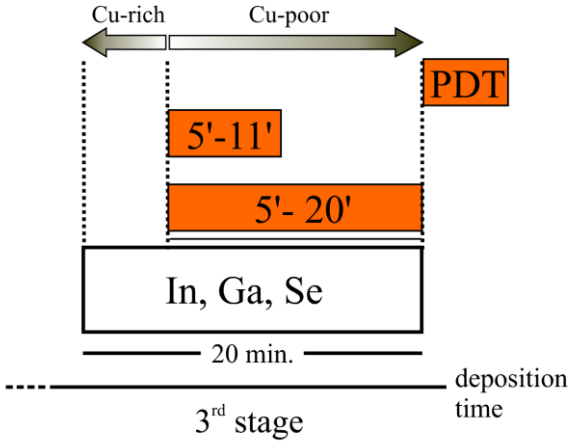

Figure 1: Schematics showing the 3rd stage of CIGS deposition with two NaF co-evaporation windows indicated as boxes. Additionally the post deposition treatment (PDT) is shown where NaF is evaporated after CIGS deposition at reduced substrate temperature of ~350°C.

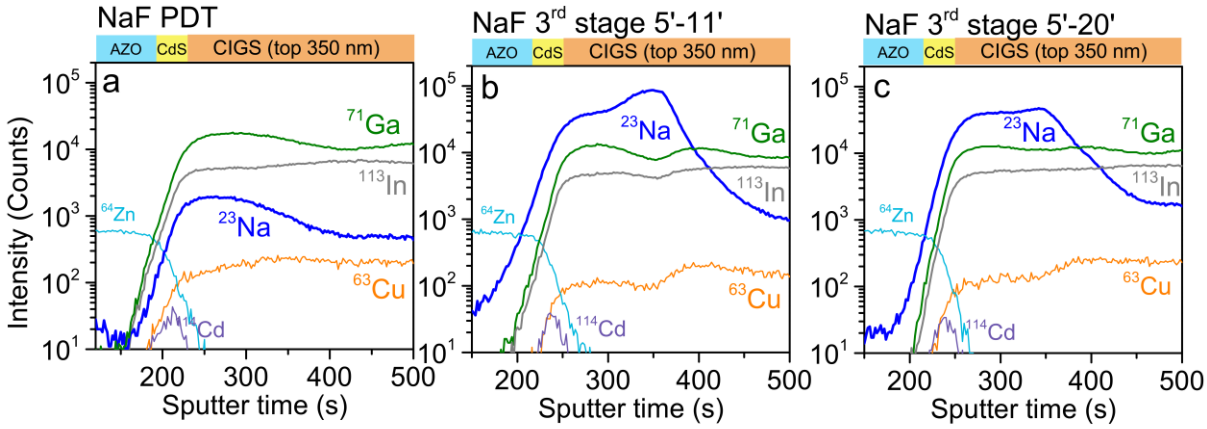

Fig. 2: SIMS depth profiles showing the top ~350 nm of the absorber for the samples with different Na introduction strategies. The time intervals of Na introduction are closely reflected in the SIMS profiles. Cu, In and Ga signals are locally reduced where Na yield increases.

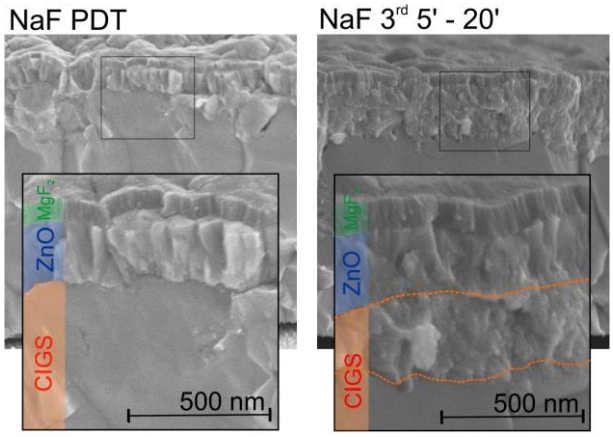

182

183 Figure 3: SEM micrograph of the samples where Na was introduced by a PDT (left) and where it was

184 co-evaporated from 5 to 20 minutes during the 3rd deposition stage (right). The region between the

185 dashed lines corresponds to the NaF co-evaporation time window and shows reduced grain size

186 compared to the PDT treated absorber.

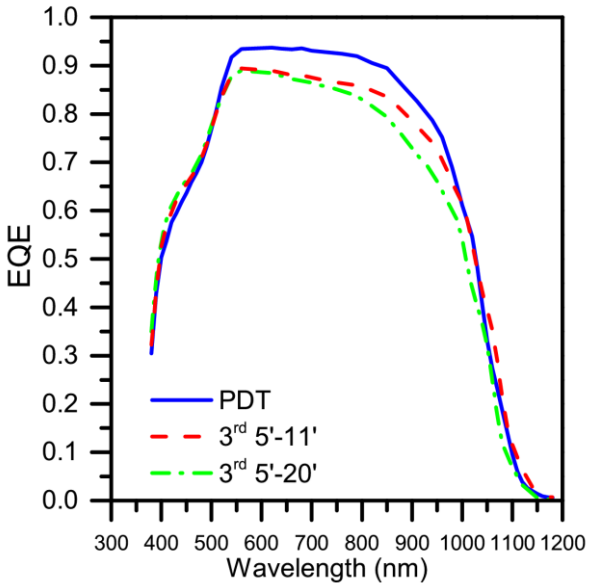

187

188 Figure 4: EQE curves of the samples with different Na introduction strategies. NaF co-evaporation

189 causes overall reduced collection efficiency. Increased NaF co-evaporation time especially decreases

190 the NIR response.

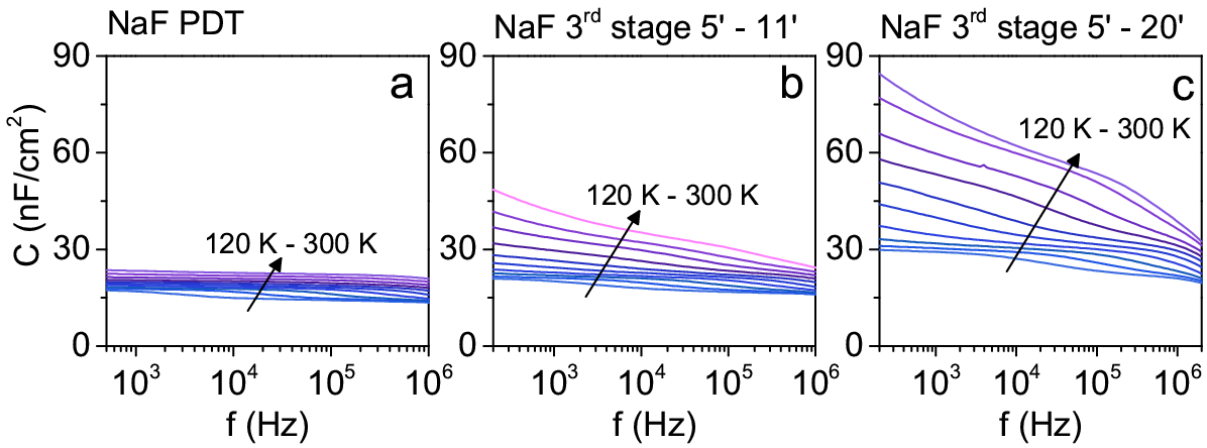

191

192 Figure 5: C-f spectra of the samples with different Na introduction strategies for temperatures

193 between 120 K and 300 K. NaF co-evaporated samples feature a more distinct capacitance step.

194

195

196 **List of tables:**

197 Table 1: Comparison of PV parameters, diode ideality factor A, reverse saturation current density j_0

198 and its activation energy E_{j0} of the different devices. Further shown are the apparent carrier density

199 N_{CV} as determined by C-V profiling and defect energies E_{def} as extracted from C-f spectra as well as

200 the Na concentrations with respect to the CIGS layer determined by ICP-MS.

201

202 **REFERENCES**

203 [1] J. Hedstrom, H. Ohlsen, M. Bodegard, A. Kylner, L. Stolt, D. Hariskos, M. Ruckh, H.W. Schock,

204 ZnO/CdS/Cu(in,Ga)Se2 Thin-Film Solar-Cells with Improved Performance, Conference Record of the

205 Twenty Third IEEE Photovoltaic Specialists Conference - 1993, (1993) 364-371.

206 [2] D. Rudmann, G. Bilger, M. Kaelin, F.J. Haug, H. Zogg, A.N. Tiwari, Effects of NaF coevaporation on

207 structural properties of Cu(In,Ga)Se2 thin films, Thin Solid Films, 431 (2003) 37-40.

208 [3] P. Salome, V. Fjallstrom, A. Hultqvist, M. Edoff, Na Doping of CIGS Solar Cells Using Low Sodium-
209 Doped Mo Layer, IEEE J. Photovolt., 3 (2013) 509-513.

210 [4] D. Rudmann, D. Bremaud, H. Zogg, A.N. Tiwari, Na incorporation into Cu(In,Ga)Se2 for high-
211 efficiency flexible solar cells on polymer foils, J. Appl. Phys., 97 (2005) 084903.

212 [5] D. Guettler, A. Chirilă, S. Seyrling, P. Blosch, S. Buecheler, X. Fontane, V. Izquierdo-Roca, L. Calvo-
213 Barrio, A. Perez-Rodriguez, J.R. Morante, A. Eicke, A.N. Tiwari, Influence of NaF Incorporation during
214 Cu(In,Ga)Se2 Growth on Microstructure and Photovoltaic Performance, 35th IEEE Photovoltaic
215 Specialists Conference, (2010) 3420-3424.

216 [6] R. Caballero, C.A. Kaufmann, T. Eisenbarth, M. Cancela, R. Hesse, T. Unold, A. Eicke, R. Klenk, H.W.
217 Schock, The influence of Na on low temperature growth of CIGS thin film solar cells on polyimide
218 substrates, Thin Solid Films, 517 (2009) 2187-2190.

219 [7] S. Puttnins, S. Levcenco, K. Schwarzburg, G. Benndorf, F. Daume, A. Rahm, A. Braun, M.
220 Grundmann, T. Unold, Effect of sodium on material and device quality deposited Cu(In,Ga)Se2, Sol.
221 Energ. Mat. Sol. C, 119 (2013) 281-286.

222 [8] A. Chirilă, P. Reinhard, F. Pianezzi, P. Bloesch, A.R. Uhl, C. Fella, L. Kranz, D. Keller, C. Gretener, H.
223 Hagendorfer, D. Jaeger, R. Erni, S. Nishiwaki, S. Buecheler, A.N. Tiwari, Potassium-induced surface
224 modification of Cu(In,Ga)Se2 thin films for high-efficiency solar cells, Nat Mater, 12 (2013) 1107-
225 1111.

226 [9] P. Jackson, D. Hariskos, R. Wuerz, W. Wischmann, M. Powalla, Compositional investigation of
227 potassium doped Cu(In,Ga)Se2 solar cells with efficiencies up to 20.8%, Phys. Status Solidi RRL, 8
228 (2014) 219-222.

229 [10] F. Pianezzi, P. Reinhard, A. Chirilă, B. Bissig, S. Nishiwaki, S. Buecheler, A.N. Tiwari, Unveiling the
230 effects of post-deposition treatment with different alkaline elements on the electronic properties of
231 CIGS thin film solar cells, Phys. Chem. Chem. Phys., 16 (2014) 8843-8851.

232 [11] F. Pianezzi, P. Reinhard, A. Chirilă, S. Nishiwaki, B. Bissig, S. Buecheler, A.N. Tiwari, Defect
233 formation in Cu(In,Ga)Se2 thin films due to the presence of potassium during growth by low
234 temperature co-evaporation process, J. Appl. Phys., 114 (2013) 194508.

235 [12] A. Chirilă, S. Buecheler, F. Pianezzi, P. Bloesch, C. Gretener, A.R. Uhl, C. Fella, L. Kranz, J.
236 Perrenoud, S. Seyrling, R. Verma, S. Nishiwaki, Y.E. Romanyuk, G. Bilger, A.N. Tiwari, Highly efficient
237 Cu(In,Ga)Se2 solar cells grown on flexible polymer films, Nature Materials, 10 (2011) 857-861.

238 [13] V. Nadenau, U. Rau, A. Jasenek, H.W. Schock, Electronic properties of CuGaSe2-based
239 heterojunction solar cells. Part I. Transport analysis, J. Appl. Phys., 87 (2000) 584-593.

240 [14] O. Cojocaru-Miredin, P. Choi, R. Wuerz, D. Raabe, Atomic-scale distribution of impurities in
241 CuInSe2-based thin-film solar cells, Ultramicroscopy, 111 (2011) 552-556.

242 [15] E. Cadel, N. Barreau, J. Kessler, P. Pareige, Atom probe study of sodium distribution in
243 polycrystalline Cu(In,Ga)Se2 thin film, Acta Mater, 58 (2010) 2634-2637.

244 [16] T. Eisenbarth, T. Unold, R. Caballero, C.A. Kaufmann, H.W. Schock, Interpretation of admittance,
245 capacitance-voltage, and current-voltage signatures in Cu(In,Ga)Se2 thin film solar cells, J. Appl.
246 Phys., 107 (2010) 034509.

247 [17] T. Walter, R. Herberholz, C. Muller, H.W. Schock, Determination of defect distributions from
248 admittance measurements and application to Cu(In,Ga)Se2 based heterojunctions, J. Appl. Phys., 80
249 (1996) 4411-4420.

250 [18] L.E. Oikkonen, M.G. Ganchenkova, A.P. Seitsonen, R.M. Nieminen, Effect of sodium
251 incorporation into CuInSe2 from first principles, J. Appl. Phys., 114 (2013) 083503.

252 [19] J. Pohl, K. Albe, Intrinsic point defects in CuInSe2 and CuGaSe2 as seen via screened-exchange
253 hybrid density functional theory, Phys. Rev. B, 87 (2013) 245203.

254 [20] U. Rau, H.W. Schock, Electronic properties of Cu(In,Ga)Se2 heterojunction solar cells-recent
255 achievements, current understanding, and future challenges, Appl. Phys. A, 69 (1999) 131-147.

256

257